ADVANCED BIOLOGY
www.advanced-bio.com

Sars-Cov-2 Spike Protein-Induced Damage of hiPSC-Derived Cardiomyocytes

Xiaochen Huang, Boxin Huang, Yong He, Liang Feng, Jian Shi, Li Wang, Juan Peng, and Yong Chen**

Sars-Cov-2 may trigger molecular and functional alterations of cardiomyocytes (CMs) of the heart due to the presence of receptor angiotensin-converting enzyme 2 (ACE2) of the host cells. While the endocytic itinerary of the virus via cleavage of the spike protein of Sars-Cov-2 is well understood, the role of the remaining part of the spike protein subunit and ACE2 complex is still elusive. Herein, the possible effects of this complex are investigated by using synthetic spike proteins of Sars-Cov-2, human-induced pluripotent stem cells (hiPSC), and a culture device made of an arrayed monolayer of cross-linked nanofibers. hiPSCs are first differentiated into CMs that form cardiac tissue-like constructs with regular beating and expression of both ACE2 and gap junction protein Connexin 43. When incubated with the spike proteins, the hiPSC-CMs undergo a rhythmic fluctuation with overstretched sarcomere structures and dispersed gap junction proteins. When incubated with the spike proteins and supplementary angiotensin II, the damage of the spike protein on hiPSC-CMs is enhanced due to downregulated ACE2, chromatin margination, altered Connexin 43 expression, sarcomere disruption, and beating break. This discovery may imply latent effects of the spike proteins on the heart.

1. Introduction

The symptoms of COVID-19 could be associated with injury and dysfunction of multi-organs, including lung, heart, blood vessels, kidney, gut, and brain[1–6] for which all studies attribute the infection to the binding of the spike protein of Sars-Cov-2 and the receptor angiotensin-converting enzyme 2 (ACE2) of the host cells.[7] While the endocytic itinerary of the virus after cleavage of the spike protein is well understood, the role of the remaining part of the spike protein subunit 1 and ACE2 complex (spike-ACE2 complex) is still elusive. Indeed, in vitro models have shown systematically an overactive immune response of the cells to Sars-Cov-2[8] but less has been devoted to the effect of the spike-ACE2 complex.

The endocytosis of the virus is initiated with a two-step cleavage on the cell membrane with help of Furin and TMPRSS2 surface proteins.[9] After a membrane fusion, the virus is endocytosed and replicated in the cytoplasm, while the spike-ACE2 complex remains on the cell membrane (**Figure 1**A). Intuitively, the spike-ACE2 complexes could have three possible ends: 1) endocytosed into the cytoplasm; 2) total or partial shed from cell membrane; 3) stay on the cell membrane. Previous studies have shown that the spike protein could be endocytosed by clathrin mediation due to its ACE2-dependence.[10] The spike protein-induced downregulation of ACE2, activation of several signaling pathways, and inflammation could also be observed.[11,12]

The objective of the present study is to investigate whether the spike protein alone, outside the context of infectious virus, can trigger molecular and functional alterations in cardiac complications that occur in 20% to 44% of hospitalized patients, and constitute an independent risk factor for COVID-19 mortality.[13–17] Human-induced pluripotent stem cells (hiPSC) are used for differentiation toward hiPSC-cardiomyocytes (CMs) with an arrayed nanofiber membrane (culture patch).[18] The derived hiPSC-CMs (cardiac patch) are then incubated with synthetic spike proteins in the presence or absence of supplementary Angiotensin II (Ang II). It is known that Ang II is the main effector of renin-angiotensin system (RAS) that can be converted by ACE2 to Angiotensin 1–7 (Ang 1–7), while Ang 1–7 has opposite cardiovascular and inflammatory effects to Ang II.[19] The presence of supplementary Ang II is meaningful to modulate the effect of spike protein in terms of RAS abnormality.[20] As a first step for screening phenotypes, the spike protein-induced rhythmic changes of hiPSC-CMs are analyzed. Then, the deviations of sarcomere structure of the cells are quantified with α-actinin and troponin T markers. Furthermore, the alternations of cytoskeleton and gap junctions are examined with actin and connexin 43 markers. These observations illustrate structural and functional damage effects of Sars-Cov-2 spike protein on hiPSC-CMs, which are consistent with current efforts in this area.

X. Huang, B. Huang, Y. He, L. Feng, J. Peng, Y. Chen
École Normale Supérieure-PSL Research University, Département de Chimie, Sorbonne Universités-UPMC Univ Paris 06, CNRS UMR 8640, PASTEUR, 24, rue Lhomond
Paris 75005, France
E-mail: juan.wang@ens.psl.eu; yong.chen@ens.psl.eu
J. Shi, L. Wang
MesoBioTech, 231 Rue Saint-Honoré
Paris 75001, France

The ORCID identification number(s) for the author(s) of this article can be found under https://doi.org/10.1002/adbi.202101327.

DOI: 10.1002/adbi.202101327

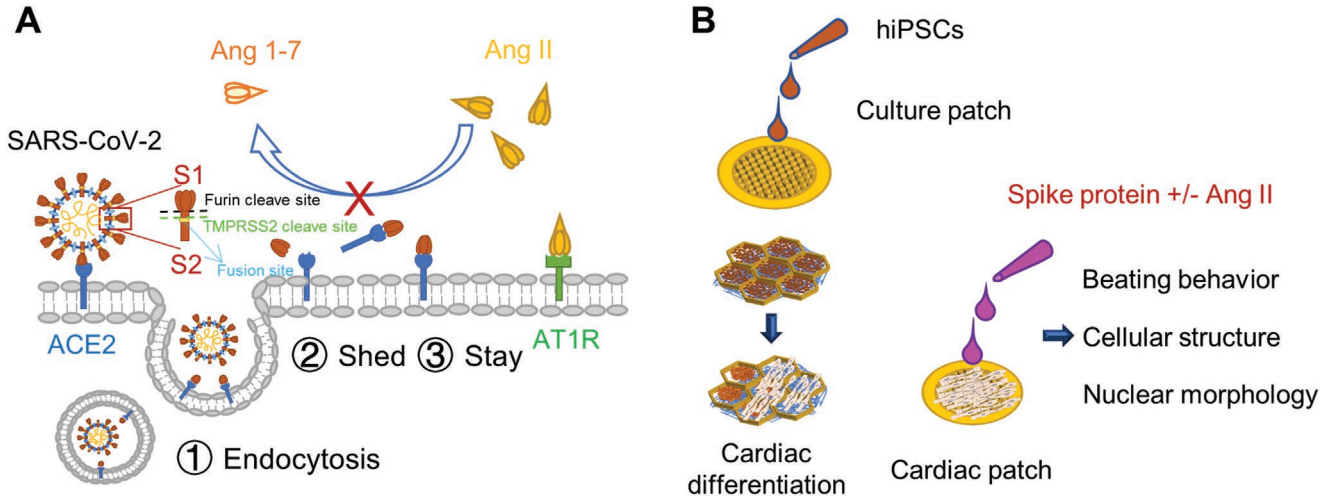

Figure 1. Overview of possible ends of shedding spike protein and evaluation process. A) After endocytosis of Sars-Cov-2, the spike-ACE2 complex may: 1) Enter into the cytoplasm; 2) Totally or partially shed from the cell membrane; 3) Stay on the cell membrane. B) Workflow of cardiac patch fabrication and spike protein testing. hiPSCs are first differentiated to cardiomyocytes on a culture patch made of arrayed nanofiber membrane. They are then incubated with synthetic spike protein with or without supplementary Ang II. The beating behavior, cellular structure, and nuclear morphology of the cells are analyzed to evaluate the effect of the spike protein of Sars-Cov-2.

2. Results

2.1. Beating and Structure of hiPSC-CMs

The culture devices (patch) used in this work for hiPSC-CMs differentiation were produced by lithography, electrospinning, and chemical crosslinking techniques.[18] The characteristics of the nanofiber patches are summarized in Figure S1 (Supporting Information), including the porosity, the average diameter of the nanofibers, permeability, and stiffness of the nanofiber membrane, together with SEM pictures to illustrate the morphology of the nanofiber membrane. Statistically, the size of 98% of pores was smaller than 7 µm, on which cells can stay without falling down. By measuring the flow rate of DI water across the membrane as a function of pressure, a membrane permeability of 3.44×10^3 nm^2 could be deduced, which is much larger than that of the commonly used etch ion tracking membrane.[21] By measuring the deflection as a function of pressure, an effective Young's modulus of the membrane in the order of 4 MPa could be obtained.[22] Accordingly, an effective in-plane Young's modulus in the order of 9.5 kPa could be estimated by using a nanofiber diameter of 0.4 µm, pore size of 6 µm, and curve fitting based on a theory of cellular solids.[23] Such an effective Young's modulus is well-suited to support hiPSC-CM differentiation.[24] Finally, the cell adhesion strength was evaluated with a spinning technique, showing a better attachment of the cells on nanofibers than on glass substrates.[25]

To generate hiPSC-CMs, the standard differentiation protocol was used[18] (**Figure 2**A). hiPSCs were first seeded on the nanofiber patch to form dome-like hiPSC colonies and then differentiated to cardiomyocytes in each of the membrane areas (Figure S2, Supporting Information). During the first 7 days, the hiPSC colonies became flat due to cardiac mesoderm induction. Starting from Day 9, 1–5% of hexagonal areas started beating slowly. The percentage of beating areas increased to 20% on day 15 and to 80% on day 64 (Movie S1, Supporting Information). Meanwhile, the beating rate of the hiPSC-CMs increased from 65 ± 13 bpm on day 15 to 153 ± 4 bpm on day 64 (Figure 2B) by analyzing the time-lapse images with a MATLAB program.[26] By dividing the time-lapse images into 30 areas (Figure 2C), three types of beating waveforms could be identified as plotted in Figure 2D. Statistically, 26 over 30 areas (marked in green) showed regular and high magnitude beatings (plotted in green). The two areas with low magnitude beatings (marked in yellow) fell mostly in the frame area, whereas the fluctuation in beating amplitude of the two red marked areas can be attributed to the inhomogeneity of the tissue construct. Nevertheless, the beating frequency of all areas was the same.

To characterize the fabricated hiPSC-CMs, α-smooth muscle actin (SMA), a marker for smooth muscle cells and myofibroblasts,[27] and troponin T (TnT), a structural marker of cardiomyocytes, were used for immune-stained analysis. In Figure 2E, immunofluorescence images showed the expression of SMA and troponin T on the hiPSC-CMs. Clearly, the derived hiPSC-CM tissue constructs consisted of at least three types of cells (TnT+, TnT-/SMA+, and TnT-/SMA-), consistent with the previous observations.[28,29] Moreover, the cross-section views of the tissue construct in Figure 2E show that the cells in the hexagonal area were stacked to form a multilayer structure where the cells on the frame or nearby are mostly spindle-shaped TnT-SMA+ cells. Interestingly, the TnT-SMA+ cells formed a thin layer at the perimeter (top layer), TnT+ cells were localized below the TnT-SMA+ cell layer (middle layers), and no-stained cells were also found at the bottom. Schematically, the hiPSC-CM tissue construct can be divided into three layers due to tissue-like self-organization (Figure 2F). Consequently, the percentage of each cell type in three layers could be estimated (Figure 2G). Apparently, the TnT+ cells were quite homogeneously distributed in all layers, while a high percentage of TnT-SMA+ cells (17.5% ± 4.58%) were in the top layer compared to that in the middle (2.52% ± 1.82%) and the bottom (4.92% ± 3.09%) layers.

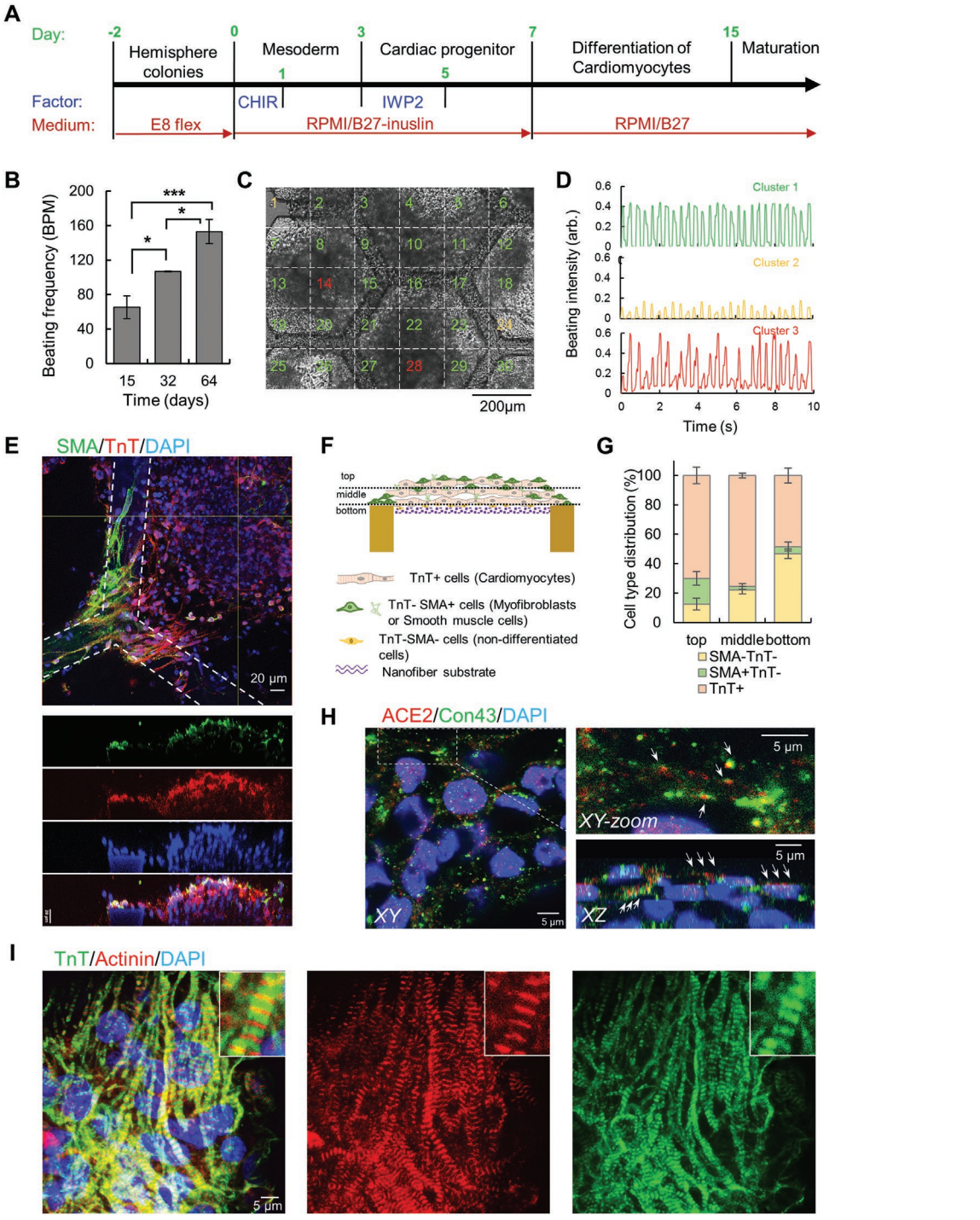

Figure 2. Fabrication and characterization of the cardiac patch. A) Timeline of hiPSC differentiation toward cardiomyocytes (CM). CHIR represents CHIR99021, a GSK3 inhibitor; IWP2 is a WNT inhibitor. B27: B27 minus insulin supplement, E8 flex: Essential 8 Flex Medium, RPMI: RPMI 1640 medium. B) Beating frequency of the hiPSC-CMs as a function of incubation time. The BPM value at each timepoint is the average of beating frequency from five positions of three independent experiments. C) Spatial segmentation of time-lapse images of mature hiPSC-CMs on day 64. D) Beating waveforms of three types of segmented areas of (C). Over 30 segmented areas, 26 exhibited regular and high magnitude beating (green). E) Immunostaining images of a selected area showing tissue-like organization with multilayer and multicellular types. The dash lines indicate the borders of the nanofiber membrane. Green: SMA (α-smooth muscle actin), Red: TnT (troponin T), Blue: Nuclei. Scale bar: 20 μm. F) Schematic of the cell organization. G) Percentages of the cells expressing TnT and/or SMA. The stack image (XZ) of (E) was divided vertically on average into three parts (top, middle, bottom shown in (F)). 10 XZ cross-section positions were analyzed. H) Immunofluorescent images of ACE2 (red) and Connexin 43 (Con43, green) marked hiPSC-CMs. Blue: Nuclei. Scale bar: 5 μm. I) Maximum intensity projection of Z-stack, fluorescence confocal image of TnT (green) and α-actinin (red) marked hiPSC-CMs. Blue: Nuclei. Scale bar: 5 μm. Zoomed areas display more clearly the sarcomere structures. Scale bar: 5 μm.

In contrast, more TnT-SMA- cells (46.72% ± 3.13%) were in the bottom layer compared to that in the top (12.5% ± 4.05%) and the middle (22.01% ± 2.54%) layers.

To evaluate the suitability of the hiPSC-CMs to the studies of the effects of spike protein, the expression levels of ACE2 and connexin 43 were analyzed. As illustrated in Figure 2H, 74.84% ± 3.05% of the cells expressed connexin 43, and 76.55% ± 3.88% of the cells expressed ACE2, some of them around the nucleus in agreement with the previous studies.[30] The sarcomere structure of the hiPSC-CMs can be seen from α-actinin and troponin T immunostained images (Figure 2I). Here, α-actinin is specific for the attachment of actin filaments to the Z-lines of the hiPSC-CMs, and troponin T is associated with the coupling between tropomyosin and actin filament. The observed period arrangement of both α-actinin and troponin T were characteristic of cardiac sarcomeres that confirmed the maturation of our hiPSC-CMs. Statically, 80.29% ± 5.33% of the troponin T were aligned in the troponin T expressed areas. Likewise, 66.11% ± 2.29% of the α-actinin formed stripy patterns in the α-actinin expressed areas.

2.2. Functional and Structural Changes of hiPSC-CMs Caused by Spike Proteins

2.2.1. Effect on the Rhythmic Behavior

The effect of the spike protein on the rhythmic activity of cardiomyocytes was studied by co-culturing the spike protein with the hiPSC-CMs. A high dosage of synthetic biotinylated spike protein (1 μg mL^{-1}) was added to the culture medium for incubation for 24 h. To track the trajectory of the spike proteins, the cells were fixed and labeled with streptavidin-594 and phalloidin-FITC for spike protein and actin filaments, respectively. The results showed striated actin structures, confirming the cardiac cell type (indicated with white arrows in **Figure 3**A). Spike proteins were found inside 88.1% ± 4.56% of the cells and they were mostly localized around the nucleus of hiPSC-CMs (Figure 3A). This means that the spike proteins partially diffused and that the striated organization of actin filaments could be affected, in agreement with the previous studies.[31]

After introducing the spike proteins, the beating frequency of the hiPSC-CMs varied. Figure 3B shows the change of normalized beating frequency over 24 h. Compared to the samples without spike protein treatment, the beating frequency of the samples with spike proteins increased during the first 3 h, then decreased until 18 h. During the last 6 h, the beating frequency of the samples with and without treatment was comparable. This result suggested that the spike protein has a limited impact on the beating frequency of hiPSC-CMs and that apparently, the cells remained alive (Movies S2 and S3, Supporting Information). We also noticed a remarkable change in the beating waveform after 18 h incubation and then a recovery at 24 h, which can be attributed to the spike protein-induced perturbation and the cellular regulation.

2.2.2. Disturbed Intracellular Structure

The spike protein-induced beating fluctuation of hiPSC-CMs may be correlated to the disturbance of sarcomere structures. The expression and distribution of α-actinin and troponin T of the samples with and without spike protein treatment were then compared (Figure 3C). Without spike protein, striated organizations of α-actinin and troponin T were observed in the immunostaining images (periodic narrow stripes in red and double stripes in green, respectively). Here, the structure of troponin T marked double stripes that represent the relaxation phase of sarcomeres was intentionally selected for comparison. With spike protein, the α-actinin associated stripes cannot be seen and the distance between the troponin T marked double stripes remarkably increased. In fact, the α-actinin proteins aggregated or diffused irregularly (Figure 3C,F), keeping the averaged intensity of α-actinin unchanged (Figure 3E). Normally, the distance between the troponin T double stripes varies with the contraction phase of the sarcomere, which is maximum when the sarcomere is completely relaxed and minimum when it is contracted. The sarcomere length (SL) of hiPSC-CMs with and without spike protein treatment could then be quantified (Figure 3D). Statistically, it varied between 0.70 and 2.17 μm for the cells without the treatment. After the spike protein treatment, 25.56% ± 7.18% of the sarcomeres have an SL showed a maximum value of 2.68 μm (Figure 3G). Since the sarcomeres are organized in the form of cross and slidable bridges of actin and myosin filaments, the excess in SL may cause of weakening of contraction ability.[32] Together, the results suggest that the spike protein impacted indeed the sarcomere structures by disrupting the organization of α-actinin and increasing the distance between the double stripes of troponin T marked structure.

2.2.3. Remodeled Gap Junction

Gap junctions are composed of connexins in the form of membrane channels, which facilitate communication between neighboring cells and thus coordinate electrical and contractile activity of the heart.[33] The spike protein-induced rhythmic change might be associated with the remodeling of the gap junctions. Therefore, the cells were immunostained with connexin 43 and actin filaments markers for visualizing the cell periphery. Without spike protein treatment, connexin 43 appeared spotty pattern on the intercellular space between cells. After the spike protein treatment, connexin 43 was aggregated around the nucleus (Figure 3H,I). Statistically, 74.19% ± 3.45% of the cells expressed connexin 43 in the perinuclear areas after the spike protein treatment (Figure 3J), suggesting an induced remodeling of the gap junction due to alternation of the connexin 43 expression caused by endocytosis.[34]

2.3. Damages Caused by Spike Protein in the Presence of Supplementary Ang II

2.3.1. Beating Arrest of hiPSC-CMs

The changes of hiPSC-CMs caused by the spike protein may be related to the alternation of the available ACE2. By coculture of hiPSC-CMs and spike proteins with supplementary Ang

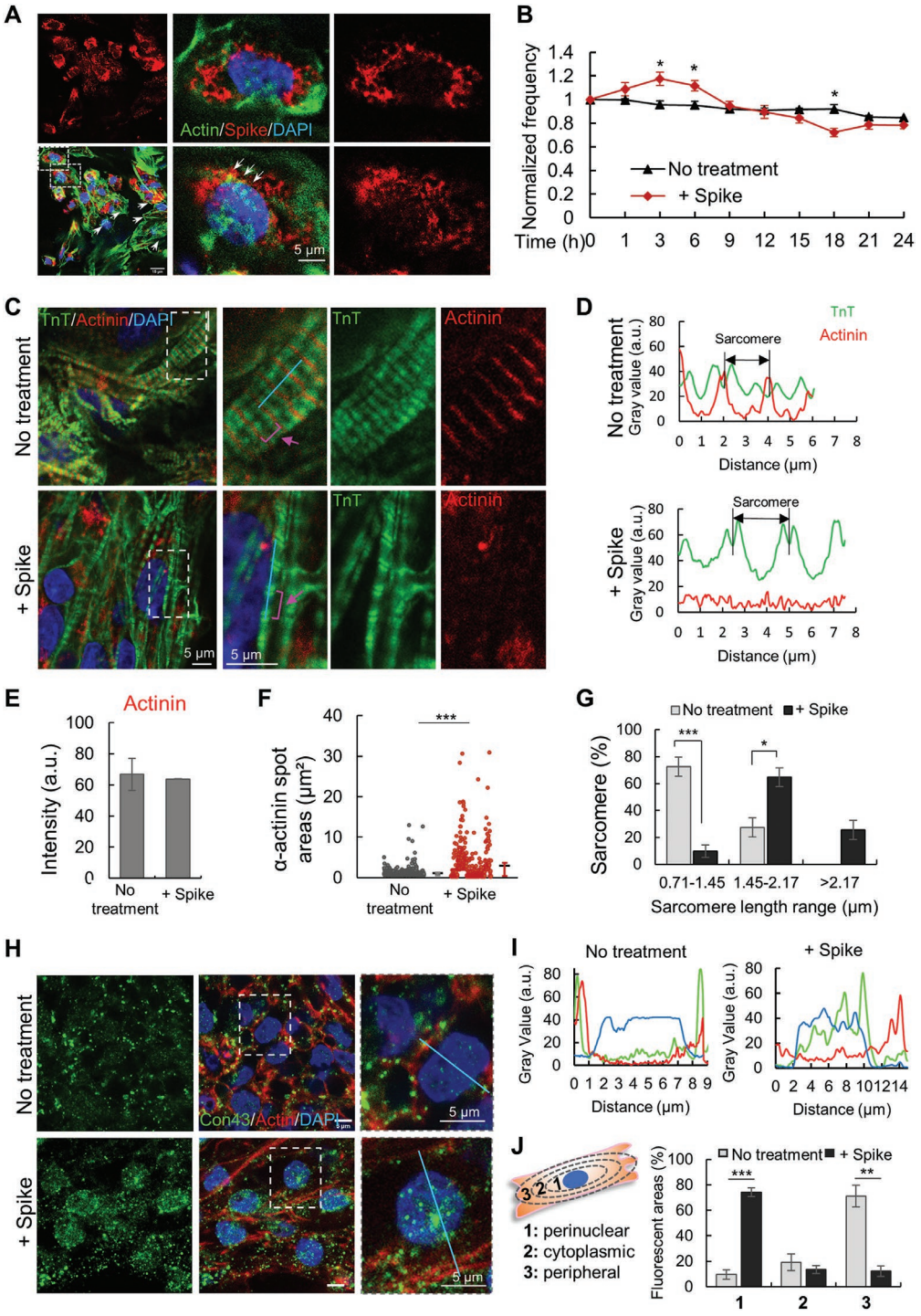

Figure 3. Effect of spike protein on hiPSC-CMs. A) Immunofluorescent images of actin (green) and spike protein (red) marked hiPSC-CMs. Blue: Nuclei. Scale bar: 15 μm. Two zoomed areas show the spike protein around the nuclei (up) and in the cytoplasm (bottom). White arrows indicate the striated structure of sarcomeric actin. Scale bar: 5 μm. B) Beating frequency variation as a function of incubation time during the first 24 h. The normalized frequency was the average one from five positions. C) Immunofluorescent images of TnT (green) and α-actinin (red) marked hiPSC-CMs. Magenta symbols indicate sarcomere structures with and without spike protein treatment, showing different lengths between neighboring TnT segments. Scale bar: 5 μm. D) Intensity profiles of TnT (green) and α-actinin (red) fluorescence along cyan lines in (C). E) Mean intensity of α-actinin fluorescence from cells of eight different positions per condition. F) The graph shows the distribution of the α-actinin spot area from cells of ten different positions. G) Statistic of the sarcomere length of in untreated and spike protein treated hiPSC-CMs. Two hundred fifty-two sarcomeres of cells from 12 different positions per condition were analyzed. H) Immunofluorescent images of connexin 43 (green) and actin (red) marked cells. Blue: Nuclei. Scale bar: 5 μm. I) Intensity profiles of connexin 43 (green) and actin (red) fluorescence along cyan lines in (H). J) Percentage of connexin 43 fluorescent areas in different zones as defined on the left. 50 cells from five different positions per condition were analyzed.

II, we observed a significant change of cell vitality. To have a striking effect, a high dosage of Ang II (100 ng mL^{-1}) was added to the culture medium after incubation for 3 h with or without the spike proteins. After incubation for 48 h, the medium was refreshed without spike protein and Ang II.

Figure 4A shows a comparison of the normalized beating frequency as a function of time over 54 h of three samples with and without the spike protein and Ang II treatment. Apparently, the hiPSC-CMs without the spike protein treatment remain alive, even a relatively high dose of Ang II was used. The beating frequency of the hiPSC-CMs treated with Ang II increased in the first 6 h and then decreased smoothly in the following 18 h. Afterward, the beating frequency of the samples with and without Ang II treatment varied in a similar manner, suggesting that the damaging effect of Ang II on the beating activity of the hiPSC-CMs is limited and that the cells remain alive after moving the Ang II. In contrast, the spike protein treatment with supplementary Ang II caused a fatal change in the rhythmic activity of the hiPSC-CMs. As can be seen, the variation of the beating frequency during the first 29 h is comparable to that of the sample treated with Ang II. Then, the beating frequency gradually decreased and the cardiac beating completely stopped in the end even after renewing the medium (Movies S4–S6, Supporting Information). This can be considered as direct evidence of the damaging effect of the spike proteins on hiPSC-CMs in the presence of supplementary Ang II.

2.3.2. Altered Nuclear Morphology

The beating arrest of hiPSC-CMs caused by spike protein with supplementary Ang II may partially be due to disturbance of the ACE2 expression. Figure 4B shows immunofluorescent staining images of ACE2 under different culture conditions, indicating a variation in ACE2 expression. In the presence of spike protein and Ang II, the intensity of ACE2 marked fluorescence was significantly lower than that without the spike protein (Figure 4C).

The effect of the spike protein on hiPSC-CMs in the presence of Ang II was further analyzed by observing the nuclear morphology. Typically, the DAPI staining images show three types of nuclear morphology as illustrated in Figure 4D: 1) chromatin diffusion homogenously in the nucleus; 2) the nucleus is split into multiple small pieces (nuclear fragmentation); 3) chromatin condenses as clusters at the edge of the nuclear membrane (chromatin margination). Compared to the samples without treatment, the presence of Ang II or spike protein with Ang II increased the percentage of nuclei having nuclear fragmentation comparably (Ang II/No treatment: ≈2.83 times; Spike protein + Ang II/No treatment: ≈3.43 times). While unlike the samples with no treatment or treated with Ang II, half of the nuclei (53.70% ± 4.0%) treated with spike protein and Ang II appeared chromatin margination. Nuclear fragmentation appears during both necrosis and apoptosis, while chromatin margination is a typical symbol of apoptosis.[35] This result suggested spike protein may cause cell death through apoptosis consistent with the finding reported before.[13]

2.3.3. Disrupted Sarcomere and Impaired Expression of Connexin 43

The spike protein with Ang II-stopped beating of hiPSC-CMs may be related to the disruptions of sarcomere structures and intracellular connection. **Figure 5**A indicates that the immunostaining of troponin T and α-actinin varied depending on the treatment. Compared to the samples without treatment, consistently these proteins kept assembling regularly as striated structures in most cells incubated with Ang II. While with the treatment of spike protein and Ang II, the specific organization of troponin T and α-actinin to represent sarcomere was changed to random distribution in most of the cells. Figure 5B shows the statistical plots of the mean intensity of troponin T and α-actinin fluorescence of the samples. With the treatment of spike protein in the presence of Ang II, the expression level of both troponin T and α-actinin was lower than that of the two other samples. Likewise, Figure 5C shows the fluorescent area of troponin T and α-actinin of the sample after spike protein and Ang II treatment, indicating a remarkable variation compared with the two other samples. In other words, the regular striated distribution of the troponin T and α-actinin became a sparse random distribution. This suggests that the supplementary Ang II aggravates the effect of the spike protein on sarcomere structure from overstretched troponin T bands to randomly distributed ones. Accordingly, the expression level of connexin 43 in the hiPSC-CMs incubated with spike protein and Ang II was significantly lower than that without spike protein treatment, due to the altered cytoskeleton and the absence of sarcomere structures (Figure 5D,E).

3. Discussion

COVID-19 pandemic has already lasted for more than two years with the emergence of several Sars-Cov-2 variants due to spike protein mutations. Expanded research is necessary to develop new models and to improve our understanding of Sars-Cov-2 infection mechanisms. In this regard, in-vitro modeling of the virus-host interaction by using hiPSC-derived tissue-like constructs could be significant. Amongst other tissue types, hiPSC-CM based modeling is specific due not only to its availability[36–40] but also to the simplicity of its damage observation, as shown in this work. Previously, we have shown that the response of hiPSC-CMs to external stimuli is substrate stiffness dependent and that hiPSC-CMs on a substrate of stiffness of ≈9 kPa are more sensitive to electric stimulation.[24] The present study was based on a culture device with an effective in-plane Young's modulus of the same order. We also found a tissue-like cell organization of hiPSC-CMs with 77.47% of CMs (Troponin T+ cells), 15.77% of myofibroblasts (SMA+ cells), and 6.76% of troponin T- and SMA- cells on our nanofiber patch. While the majority of myofibroblasts were localized on the top of the tissue-like structure, the troponin T- and SMA-cells were mostly on the bottom of the structure. These cells are mostly stromal cells but some of them could be undifferentiated cells. Moreover, a few pace making cells may be enough to induce beating, with the faster cells over-riding quiescent cells. This discovery shows the tissue-like features in the presence of myofibroblasts could be improved in a similar way to that observed in

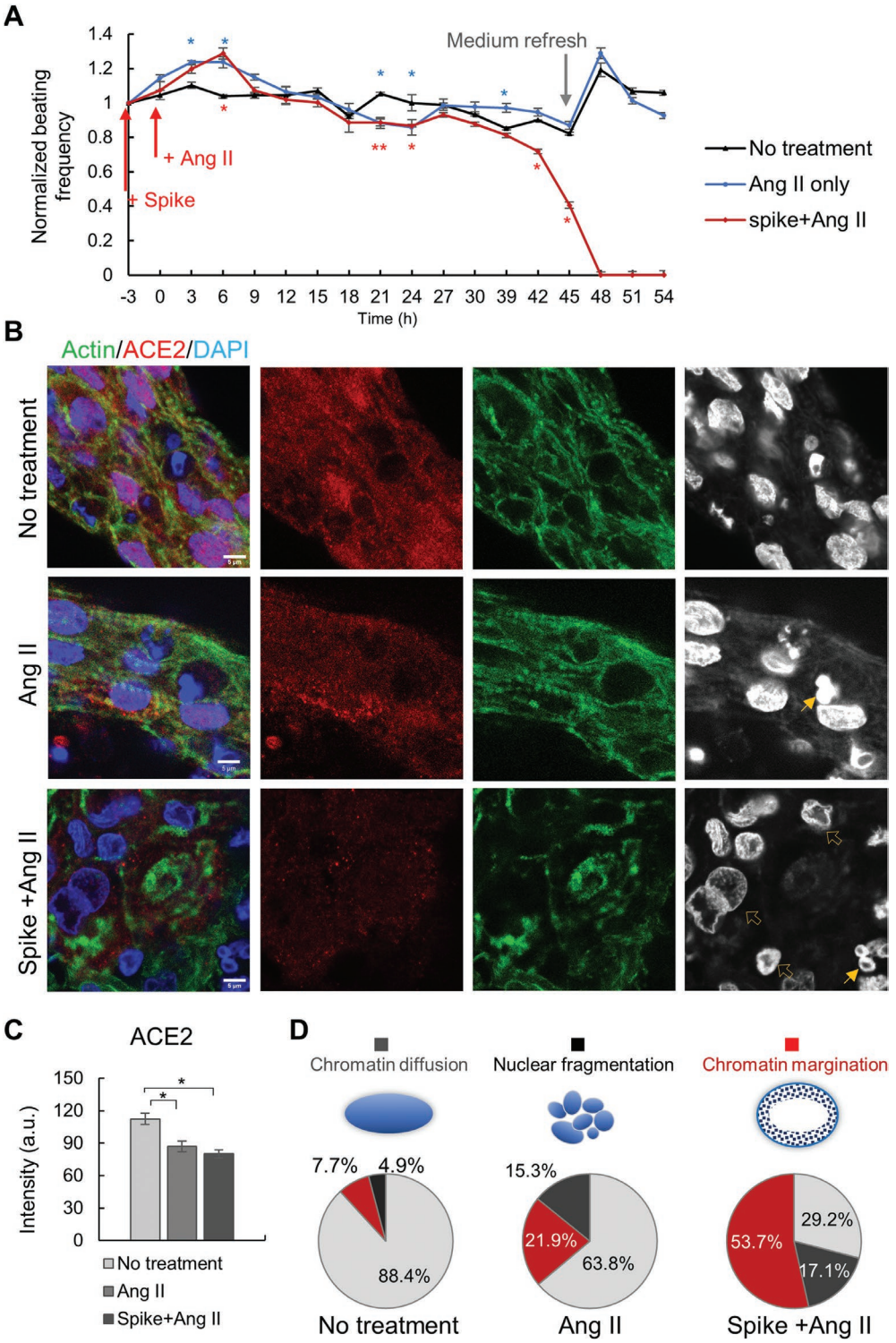

Figure 4. Beating arrest and nuclear distortion of hiPSC-CMs. A) Comparison of the rhythmic activity of hiPSC-CMs incubated for 54 h, with or without spike protein and Ang II. Spike protein (1 µg mL^{-1}) was added at –3 h, 100 ng mL^{-1} Ang II was added after another 3 h. Data were obtained from five positions under each condition. The blue and red significant symbols indicate the difference of the group "Ang II only/No treatment" and the group "Spike+Ang II/No treatment," respectively. B) Immunofluorescent images of hiPSC-CMs, showing expression of ACE2 (Green), Actin (Red) and Nucleus (Gray or Blue) under different conditions. Yellow full arrows point to cells with nuclear fragmentation while yellow hollow arrows point to cells with chromatin margining. Scale bar: 5 µm. C) The bar graph shows the mean intensity of ACE2 fluorescence from cells of 8 different positions. D) Schematic figures to show different nuclear morphology and data statistical analyses, showing quantitatively the changes in chromatin distribution. The nuclei of 120–150 cells from ten positions per condition were analyzed.

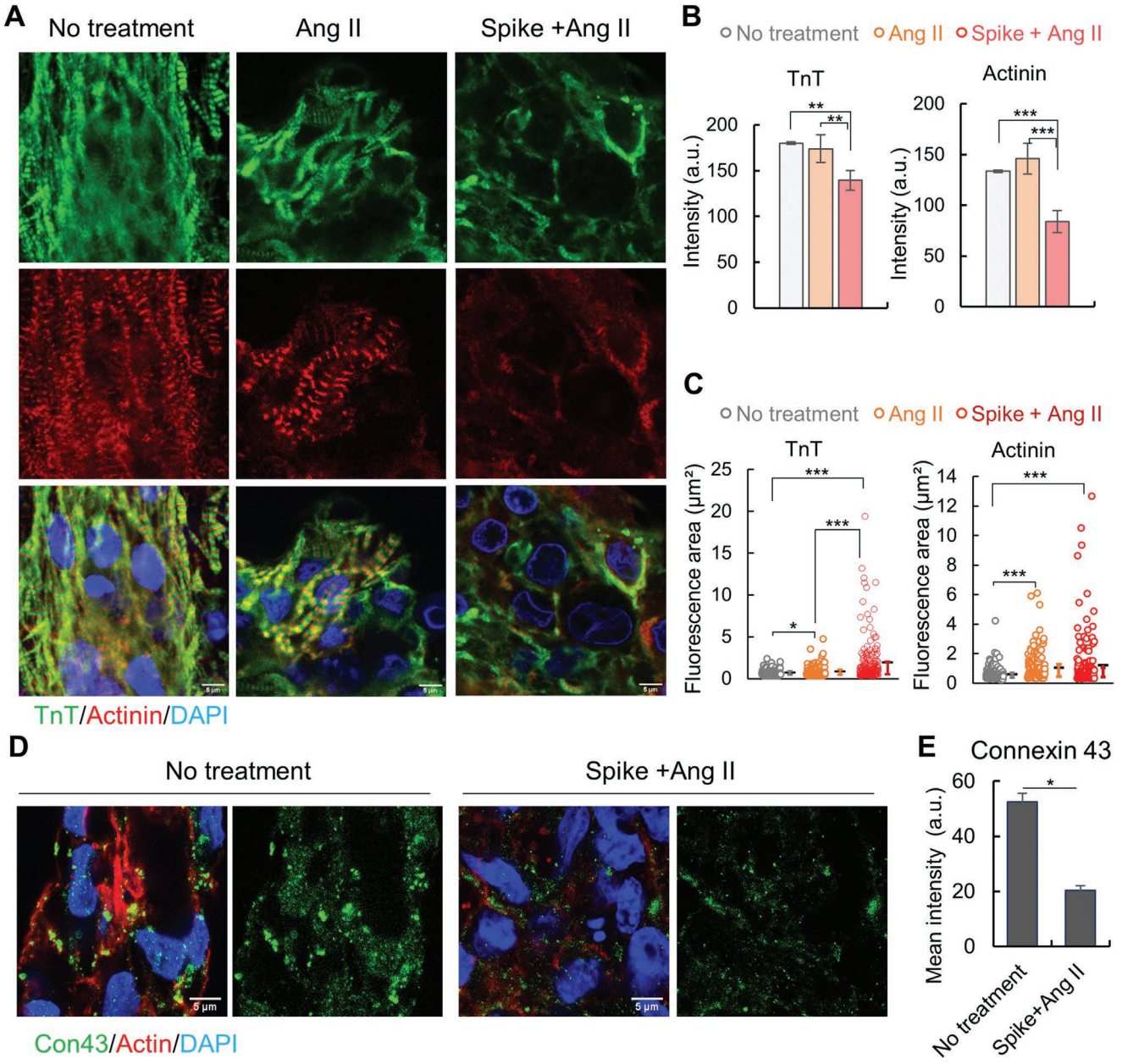

Figure 5. Degradation of the cellular structures of hiPSC-CMs. A) Immunofluorescent images of hiPSC-CMs, showing the expression of TnT (Green), Actinin (Red) under different conditions. Scale bar: 5 μm. B,C) Bar graphs at left show the mean intensity of TnT (B) and Actinin (C) fluorescence, bar graph at right shows the distribution of TnT (B) and Actinin (C) fluorescence spot areas with no treatment, spike protein or spike protein, and supplementary Ang II. D) Immunostaining images of connexin 43 (Green) and Actin (Red). Scale bar: 5 μm. E) Mean intensity of the connexin 43 fluorescence. All the data of α-actinin, troponin T, or connexin 43 were from five different positions per condition.

hiPSC-derived cardiac spheroids.[41] Compared to other engineering techniques,[38–42] the suspended culture of hiPSC-CMs has additional advantages of easy stiffness regulation and a higher degree of mini tissue-like self-organization.

By using hiPSC-CMs with tissue-like features, we were able to demonstrate the structural and functional damage effects of synthetic Sars-Cov-2 spike proteins that are schematically summarized in **Figure 6**, including i) sarcomere structure, ii) connexin 43 distribution, and iii) chromatin phenotype. The functional consequence of these structural changes was the variation of the rhythmic activities, including desynchronization and beating frequency fluctuation without supplementary Ang II and beating stop with supplementary Ang II.

Synthesized biotinylated spike proteins of 1 μg mL^{-1} (37×10^{-9} M) concentration were used. The number of spike proteins per milliliter at this dosage is $\approx 2 \times 10^{13}$, which is significantly larger than the available ACE2 receptors for a total cell number of 10^6. Experimentally, this dosage was sufficiently high for the observation of the effect of spike protein-mediated cell signaling.[12] Nevertheless, cells in culture could still

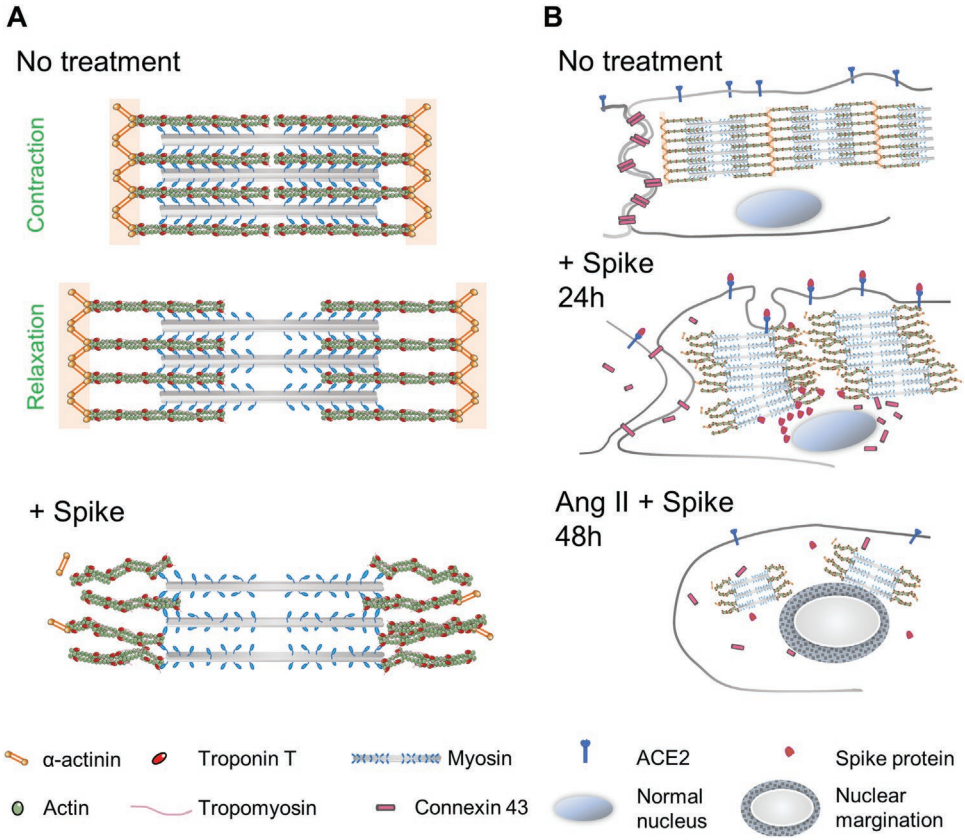

Figure 6. Schematic summaries of the effects of spike protein on hiPSC-CMs. A) Sarcomere structures with and without spike protein treatment. Without spike protein, myosin slides along actin to contract the hiPSC-CMs. With spike protein, the distribution of α-actinin proteins might be disturbed and the overlap between myosin and actin became shortened. B) Damage effects of the spike protein on cells. Without spike protein, the cell-cell contact with the help of gap junction proteins (connexin 43) enables coordinated contraction of the cardiac tissue. With spike protein, the gap junction disappeared due to mislocalization of connexin 43. When incubated with supplementary Ang II, the spike protein-induced changes became fatal in terms of ACE2 downregulation, chromatin margination, connexin 43 expression, and sarcomere disruption, leading to cell death.

be alive when the spike protein was used alone. Clinically, the free spike protein could be detected from the serum samples of COVID-19 patients in the range of 2.5–17.5 μg mL^{-1},[43] which is much higher than the concentration we used. Therefore, the testing concentration of the spike proteins would mimic the minimal effect of free spike protein on cells. On the other hand, the dosage of Ang II we used was about 100 times higher than that of the physiological and pathological conditions.[44] However, our data suggested that the Ang II alone at this high dosage has a much less injury effect than that of the combined use with the spike proteins.

The spike protein interacts with ACE2 through its RBD site. As illustrated in Figure 1, the spike can enter into the cell, shedding or staying on the cell membrane. Whether the entry of spike proteins is through endocytosis is unclear. However, the presence of the spike proteins in the intracellular areas was demonstrated in this work (Figure 2) and others.[45] It seems that the spike proteins were mostly located near the nuclei. Although the structural changes of the cells mentioned above could be attributed to the spike proteins, the mechanisms underlying remains to elucidate. Previous studies have shown that the actin cytoskeleton rearrangement occurs due to coronavirus internalization[46] and the spike protein could bind with nonmuscle myosin in pulmonary epithelial cells.[47] In the case of hiPSC-CMs, such an attachment may cause dysfunction of the sarcomere.

The overstretched sarcomere caused by spike proteins may decrease the beating frequency and dysfunction of actin/myosin filaments or their bridging structure.[48] Furthermore, the altered localization of connexin 43 remodeled the intercellular connection, since connexin 43 is a component of gap junction localized on the cell membrane to play a crucial role in the synchronized contraction of the hiPSC-CMs. In the presence of spike proteins, connexin 43 was dispersed in the cytoplasm close to the nucleus. Consequently, the synchronized beating might be disrupted.

The decrease of ACE2 expression level due to spike protein or Sars-Cov-2 infection was previously observed.[11] The related effects on immune response, or cytokine production of the cell due to the imbalance of RAS system have also been discussed.[49] A pathological amount of Ang II (100 ng mL^{-1}) was added, which could affect cardiac beating rate and Ca^{2+} signaling pathway[50] even without spike protein. This concentration has been reported to affect cardiac activities[51] but is not fatal to cardiomyocytes.[52] Indeed, more cells underwent apoptosis and necrosis and more cells showed abnormal nuclear morphology in the

presence of Ang II. After a short period of incubation, however, the majority of the cells were alive and kept beating. The change of the cell state can be attributed to the unbalanced signalization of pro- and anti-inflammation pathways due to excess of Ang II. Indeed, Ang II can be converted by ACE2 to Ang 1–7 to activate Mas signaling pathways while unconverted Ang II mainly activates AT1R. In the case of a high dosage of Ang II, excess of Ang II occurs since the conversion rate of ACE2 is limited. Then, the AT1R-mediated signaling pathways can be over-activated, giving rise to inflammation-like behaviors of the cells. After the spike protein-treatment in the presence of supplementary Ang II, the beating of hiPSC-CMs arrested and most cells showed abnormal nuclear morphology. This can be attributed to the spike protein consumption of ACE2, which makes the conversion from Ang II to Ang 1–7 less efficient. Consequently, the AT1R-mediated signaling pathways could be even more over-activated, giving rise to more pronounced damage effects.

The presence of the spike protein in the intracellular area was previously observed when cells were infected by the coronavirus. Then, cytokine production, sarcomere disassembly, and cell death could be expected.[16] Our data provide new insights on the damage of hiPSC-CMs caused by the spike-ACE2 complex, independent from the mechanism of virus replication. Recent studies have shown that the full-length spike protein may act as a ligand to induce non-infective cellular stress by activation of the extracellular signal-regulated kinase 1/2 (ERK1/2) through the CD147 receptor in human cardiac pericytes.[53] Together, the effect of the spike protein might be significant, suggesting that adjuvant care might be necessary. More systematic investigations are expected by considering different dosages of spike protein and different concentrations of Ang II as well as antagonist drugs such as ACE2 inhibitors and AT1R-blockers. Finally, the effects of the spike-ACE2 complex released after endocytosis of Sars-Cov-2 under pathological conditions must be studied to elucidate the joint effect of the virus replication and the complex.

4. Conclusion

We reported a study of the effect of Sars-Cov-2 spike protein on hiPSC-CMs. A cardiac tissue-like construct was generated by the differentiation of hiPSCs into CMs on an arrayed monolayer of cross-linked nanofibers. Our results showed that the spike proteins alone were able to provoke a damaging effect in terms of rhythmic fluctuation overstretching of sarcomere structures, and dispersion of gap junction proteins. With supplementary Ang II, the structure and function of the hiPSC-CMs underwent drastic changes due to downregulated ACE2, chromatin margination, connexin 43 mislocalization, sarcomere disruption, and inevitably beating break. Further studies on the effect of the spike proteins shed from Sars-Cov-2 should enrich our understanding of the COVID-19 pandemic.

5. Experimental Section

Patch Fabrication: The patch was fabricated as described previously.[18] First, a hexagonal microframe with an outer ring was patterned by using two-level photolithography and vacuum-assisted UV molding techniques. The pattern was defined in a chromium mask with a micropattern generator (μPG 101, Heidelberg Instruments, Germany) and chemical etching. A photoresist layer (AZ 40XT, MicroChem, France) of 50 μm thickness was spin-coated on the mask and exposed from the backside with UV light. Afterward, a ring pattern was added by spin-coating another 50 μm photoresist layer and frontside UV-exposing. After development, the resist pattern (mold) was anti-sticking treated in trimethylchlorosilane (TMCS) vapor for 1 min. Then, a solution of polydimethylsiloxane (PDMS) was prepared by mixing PDMS pre-polymer and its cross-linker (GE RTV 615, GE, France) at a weight ratio of 10:1 and poured onto the mold. After bubble removal, PDMS was cured at 75 °C for 4 h and peeled off from the mold. Next, the PDMS replica was placed on a glass slide (pattern side in touch of the glass) for vacuum-assisted UV molding. After gas removal (5 min), a low viscous photoresist, OrmoStamp (Micro Resist Technology), was introduced to fill the cavity between PDMS and glass. After UV exposure for 120 s at 21.6 mW cm^{-2}, the solidified OrmoStamp structure (frame) was separated from the PDMS mold and the glass slide.

A monolayer of gelatin nanofibers was deposited on the frame by electrospinning and chemical crosslinking. To collect the nanofibers more uniformly, the frame was coated with Au with a sputter (K6785X, Emitech) and placed on an aluminum-covering dish (collector). Gelatin solution was prepared with 12 wt.% gelatin powder (G2625, Sigma) and a solvent mixture of DI water, ethyl acetate, and acetic acid at a volume ratio of 10:14:21. The gelatin solution was ejected at a flowrate of 0.2 mL h^{-1} at a bias voltage of 11 kV and a distance of 10 cm between the stainless-steel needle (23-gauge) of the syringe and the collector. After electrospinning, the sample was dried overnight in a desiccator to remove the residual solvent and the nanofibers were cross-linked in an ethanol solution containing 0.2 M *N*-hydroxy succinimide (NHS, Sigma) and 0.2 M 1-ethyl-3-(3-dimethylaminopropyl) carbodiimide hydrochloride (EDC, Sigma) for 4 h. Finally, the sample (patch) was washed three times in ethanol and dried in a vacuum overnight to eliminate the residual solvent.

SEM Characterization: The patch was soaked in 30% ethanol solution (in DI water) for 30 min, and dehydrated by subsequent immersion in 50%, 70%, 80%, 90%, 95%, and 100% ethanol in DI water, each for 10 min and dried with a vacuum pump. Afterward, a gold layer of 2 nm thickness was deposited with a sputter and the samples were observed by using a scanning electron microscope (SEM, Hitachi S-800, 10 kV).

Differentiation of hiPSC-CMs: hiPSCs (Human episomal line, Thermofisher Scientific) were cultured with complete Essential 8 Flex Medium (E8FM, Thermo Fisher Scientific) in a dish coated with 1:100 diluted vitronectin (A14700, Thermo Fisher) and placed in an incubator of 37 °C in 5% CO_2. The medium was refreshed every 2 days until the cells reached ≈80% confluence. Cells were then collected by dissociation with a 0.5×10^{-3} M EDTA (15575-038, Life Technologies) in DPBS. To promote the adhesion of hiPSCs on gelatin nanofibers, the patch was coated with 1:500 diluted vitronectin in DPBS and then fixed in a culture dish with a PDMS hollow cylinder. 2×10^5 hiPSCs in 500 μL E8 flex medium containing 10×10^{-6} M Y-27632 (ROCK inhibitor, Y0503, Sigma) were dropped on the culture patch through the hollow area of the cylinder and incubated for 2 h. Afterward, the hollow cylinder was removed and a fresh E8 flex medium of 2 mL without 10×10^{-6} M Y-27632 was gently added to the dish. After 48 h, hemisphere hiPSC colonies were formed for cardiac differentiation using the protocol of Lian et al.[27] Briefly, RPMI 1640 medium (21 875 034, Gibco) containing B27 minus insulin supplement (A1895601, Thermo Fisher Scientific) was used as a base medium during the cardiac differentiation. On day 0, the E8 flex culture medium was replaced by the basal medium with 12×10^{-6} M of CHIR99021 (SML1046, Sigma). It is a GSK3 inhibitor to induce mesoderm differentiation. After 24 h incubation, CHIR99021 was removed. Then cells were cultured with the basal medium for 48 h. On day 3, 5×10^{-6} M of IWP2 (I0536, Sigma), the WNT activator was added into the basal medium for cardiac mesoderm induction. On day 5, the medium was replaced with the basal medium. Then, the culture medium was replaced

by RPMI 1640 containing B27 (11 530 536, Thermo Fisher Scientific) every 2 days. Generally, cells started beating around days 8 and 10 and synchronous contraction was observed between days 21 and 30.

Incubation with Spike Protein of Sars-Cov-2 or Ang II: The recombinant biotinylated Sars-Cov-2 spike protein (bs-46003P-Biotin) and Ang II (A9525) were purchased from Bioss and Sigma. The hiPSC-CM samples of at least 60 days of differentiation were used for spike protein or Ang II treatment.

For the experiment for spike protein treating, Spike protein (1 μg mL^{-1}) was added to cardiac patch for 24 h, another group was treated with the normal medium as control. For the experiment of spike protein and Ang II treatment, the cardiac patch was treated with 1 μg mL^{-1} spike protein and 100 ng mL^{-1} Ang II under three different conditions: 1) Spike + Ang II: Spike protein treatment for 48 h, together with Ang II added after 3 h of spike protein treatment; 2) Ang II only: Ang II treatment for 48 h; 3) No treatment: normal medium culture for 48 h.

Time-Lapse Imaging and Beating Analyses: The beating videos of the cardiac patch under different conditions were captured as sequential phase-contrast images by a live cell imaging system-Muvicyte (Perkin Elmer, France) with a 10× objective at a frame rate of 20 fps, a resolution of 1396 × 1052 pixels. At least three positions on the cardiac patch were selected for further monitoring. Before any treatment, a 20 s video was captured per position as the baseline. After treatment, 20 s video was captured per 3 h for 24 or 54 h depending on the experiment. All captured videos were analyzed by a MATLAB program to acquire beating frequency and beating waveform.

To evaluate the beating frequency as a function of incubation time, the recorded time-lapse images were spatially segmented into 30 rectangle areas. The beating frequency of each area was determined and averaged over the whole image. Data obtained with an untreated hiPSC-CM sample were used as a baseline to normalize the beating frequency of treated samples for each time point. To ensure statistical relevance, data were collected from three or five randomly selected positions of each sample and then averaged before reporting.

Immunostaining Characterization: The cardiac patches were rinsed with PBS to remove detached and dead cells. Then, the patches with cells were fixed in a solution of 4% paraformaldehyde for 15 min and permeabilized in 0.5% Triton X-100 for 10 min at room temperature. For nonspecific binding blocking, cells were treated with a PBS solution containing 0.1% Tween-20, 0.1% Triton X-100, and 3% bovine serum albumin for 2 h at room temperature. Afterward, the samples were treated with primary antibodies, i.e., anti-α-actinin (Sarcomeric) antibody (1:200 diluted, Sigma, Japan), anti-Troponin T-C (1:200 diluted, Santa Cruz), anti-connexin 43 (1:100 diluted, Sigma), and anti-ACE2 (1:100 diluted, Santa Cruz) in blocking buffer overnight at 4 °C. Afterward, the samples were incubated with the corresponding secondary antibody for 2 h at room temperature. For spike protein staining, the samples were also incubated with streptavidin, Alexa Fluor 594 conjugate (1:200 diluted, Thermo Fisher) to visualize the localization of biotinylated spike protein. Then, cell nuclei were labeled with 300 ng mL^{-1} 4′-6-diamidino-2-phenylindole (DAPI) (1:100 diluted, Sigma) for 15 min, and then rinsed with PBS. Phalloidin-FITC (1:200 diluted, Sigma) or Alexa Fluor 594 (2 drops mL^{-1}, Sigma) were used to label actin filaments for 30 min when necessary. Finally, the stained samples can be observed using an LSM Zeiss 710 confocal microscope. For the fluorescent intensity analysis in each experiment, all data were analyzed by ImageJ software.

Statistic Analysis: Data were presented as mean ± standard error. The statistical differences between groups were performed using Student's *t*-test. Differences were considered statistically significant at *p*-value < 0.05 ($^{*}p < 0.05$; $^{**}p < 0.01$; $^{***}p < 0.001$). The *p*-values are indicated in the figure captions where necessary.

Supporting Information

Supporting Information is available from the Wiley Online Library or from the author.

Acknowledgements

X.H. was supported by a fellowship from China Scholarship Council. This work was supported by the Agence Nationale de la Recherche under contract No ANR-17-CE09-0017 (AlveolusMimics), DIM ELICIT program from Région Ile-de-France (AutoStemLab), and PSL-Valorization through Pre-maturation project, and IPGG Carnot.

Conflict of Interest

The authors declare no conflict of interest.

Author Contributions

X.H. performed the device preparation, hiPSC differentiation, and data acquisition. J.P. and Y.C. were involved in planning and data analyses. All authors discussed the results and commented on the manuscript.

Data Availability Statement

The data that support the findings of this study are available from the corresponding author upon reasonable request.

Keywords

ACE2, Ang II, cardiomyocytes, hiPSC, Sars-Cov-2, spike protein

Received: December 28, 2021
Revised: April 12, 2022
Published online: May 6, 2022

[1] W. J. Wiersinga, A. Rhodes, A. C. Cheng, S. J. Peacock, H. C. Prescott, Pathophysiology, T. , *JAMA* **2020**, *324*, 782.
[2] F. Maghool, A. Valiani, T. Safari, M. H. Emami, S. Mohammadzadeh, *Scand. J. Immunol.* **2021**, *93*, e12999.
[3] S. Raghavan, R. Gayathri, S. Kancharla, P. Kolli, J. Ranjitha, V. Shankar, *Front. Cardiovasc. Med.* **2021**, *8*, 670659.
[4] K. Sato, J. E. Sinclair, H. Sadeghirad, J. F. Fraser, K. R. Short, A. Kulasinghe, *Clin. Transl. Immunol.* **2021**, *10*, e1343.
[5] M. Bearse, Y. P. Hung, A. J. Krauson, L. Bonanno, B. Boyraz, C. K. Harris, T. L. Helland, C. F. Hilburn, B. Hutchison, S. Jobbagy, M. S. Marshall, D. J. Shepherd, J. A. Villalba, I. Delfino, J. Mendez-Pena, I. Chebib, C. Newton-Cheh, J. R. Stone, *Mod. Pathol.* **2021**, *34*, 1345.
[6] S. T. DeKosky, P. M. Kochanek, A. B. Valadka, R. S. B. Clark, S. H. Y. Chou, A. K. Au, C. Horvat, R. M. Jha, R. Mannix, S. R. Wisniewski, M. Wintermark, S. E. Rowell, R. D. Welch, L. Lewis, S. House, R. E. Tanzi, D. R. Smith, A. Y. Vittor, N. D. Denslow, M. D. Davis, O. Y. Glushakova, R. L. Hayes, *J. Neur.* **2020**, *38*, 1.
[7] E. Knyazev, S. Nersisyan, A. Tonevitsky, *Front. Immunol.* **2021**, *12*, 3639.
[8] K. G. Chen, K. Park, J. R. Spence, *Nat. Cell Biol.* **2021**, *23*, 822.
[9] Zhang, Q. , Xiang, R. , Huo, S. , Zhou, Y. , Jiang, S. , Wang, Q. , Yu, F. , *Signal Transduction Targeted Ther.* **2021**, *6*, 233.
[10] A. Bayati, R. Kumar, V. Francis, P. S. McPherson, *J. Biol. Chem.* **2020**, *296*, 100306.
[11] Y. Lei, J. Zhang, C. R. Schiavon, M. He, L. Chen, H. Shen, Y. Zhang, Q. Yin, Y. Cho, L. Andrade, G. S. Shadel, M. Hepokoski, T. Lei, H. Wang, J. Zhang, J. X. J. Yuan, A. Malhotra, U. Manor, S. Wang, Z.-Y. Yuan, J. Y. J. Shyy, *Circ. Res.* **2021**, *128*, 1323.

[12] Y. J. Suzuki, S. I. Nikolaienko, V. A. Dibrova, Y. V. Dibrova, V. M. Vasylyk, M. Y. Novikov, N. V. Shults, S. G. Gychka, *Vasc. Pharmacol.* **2021**, *137*, 106823.
[13] A. Sharma, G. Garcia Jr, Y. Wang, J. T. Plummer, K. Morizono, V. Arumugaswami, C. N. J. C. R. M. Svendsen, *Cell Rep. Med.* **2020**, *1*, 100052.
[14] K. Navaratnarajah Chanakha, R. Pease David, J. Halfmann Peter, B. Taye, A. Barkhymer, G. Howell Kyle, E. Charlesworth Jon, A. Christensen Trace, Y. Kawaoka, R. Cattaneo, W. Schneider Jay, E. Dutch Rebecca, *J. Virol.* **2021**, *95*, 01368.
[15] A. Perez-Bermejo Juan, S. Kang, J. Rockwood Sarah, R. Simoneau Camille, A. Joy David, C. Silva Ana, N. Ramadoss Gokul, R. Flanigan Will, P. Fozouni, H. Li, P.-Y. Chen, K. Nakamura, D. Whitman Jeffrey, J. Hanson Paul, M. McManus Bruce, M. Ott, R. Conklin Bruce, C. McDevitt Todd, *Sci. Transl. Med.* **2021**, *13*, eabf7872.
[16] A. L. Bailey, O. Dmytrenko, L. Greenberg, A. L. Bredemeyer, P. Ma, J. Liu, V. Penna, E. S. Winkler, S. Sviben, E. Brooks, A. P. Nair, K. A. Heck, A. S. Rali, L. Simpson, M. Saririan, D. Hobohm, W. T. Stump, J. A. Fitzpatrick, X. Xie, X. Zhang, P.-Y. Shi, J. T. Hinson, W.-T. Gi, C. Schmidt, F. Leuschner, C.-Y. Lin, M. S. Diamond, M. J. Greenberg, K. J. Lavine, *JACC Basic Transl. Sci.* **2021**, *6*, 331.
[17] Y. Xie, E. Xu, B. Bowe, Z. Al-Aly, *Nat. Med.* **2022**, *28*, 583.
[18] Y. Tang, L. Liu, J. Li, L. Yu, L. Wang, J. Shi, Y. Chen, *Nanoscale* **2016**, *8*, 14530.
[19] M. K. Ames, C. E. Atkins, B. Pitt, *J. Vet. Intern. Med.* **2019**, *33*, 363.
[20] M. M. Givertz, *Manipulation of the renin-angiotensin system* **2001**, *104*, 14.
[21] F. Liang, X. C. Huang, J. Peng, H. Y. Luo, J. Shi, L. Wang, Y. Chen, A microfluidic system for rapid determination of Darcy permeability of filtration membranes: from patterned micro-holes to artificial basement membranes, to be unpublished.
[22] M. Radiom, Y. He, J. Peng-Wang, A. Baeza-Squiban, J.-F. Berret, Y. Chen, *Biotechnol. Bioeng.* **2020**, *117*, 2827.
[23] L. J. Gibson, M. F. Ashby, *Cellular Solids: Structure and Properties*, 2 ed., Cambridge University Press, Cambridge, **1997**.
[24] B. Wang, X. Tu, J. Wei, L. Wang, Y. Chen, *Biofabrication* **2018**, *11*, 015005.
[25] B. Huang, J. Peng, X. Huang, F. Liang, L. Wang, J. Shi, A. Yamada, Y. Chen, *ACS Appl. Mater. Interfaces* **2021**, *13*, 55939.
[26] M. Maddah, J. D. Heidmann, M. A. Mandegar, C. D. Walker, S. Bolouki, B. R. Conklin, K. E. Loewke, *Stem Cell Rep.* **2015**, *4*, 621.
[27] A. V. Shinde, C. Humeres, N. G. Frangogiannis, *Biochim. Biophys. Acta, Mol. Basis Dis.* **2017**, *1863*, 298.
[28] X. Lian, J. Zhang, S. M. Azarin, K. Zhu, L. B. Hazeltine, X. Bao, C. Hsiao, T. J. Kamp, S. P. Palecek, *Nat. Protoc.* **2013**, *8*, 162.
[29] N. Balafkan, S. Mostafavi, M. Schubert, R. Siller, K. X. Liang, G. Sullivan, L. A. Bindoff, *Sci. Rep.* **2020**, *10*, 18498.
[30] H. I. Ahmad Mulyadi Lai, S.-J. Chou, Y. Chien, P.-H. Tsai, C.-S. Chien, C.-C. Hsu, Y.-C. Jheng, M.-L. Wang, S.-H. Chiou, Y.-B. Chou, D.-K. Hwang, T.-C. Lin, S.-J. Chen, Y.-P. Yang, *Int. J. Mol. Sci.* **2021**, *22*, 1320.
[31] J. Schneider, D. Pease, C. Navaratnarajah, P. Halfmann, D. Clemens, D. Ye, C. Kim, A. Barkhymer, S. Cohle, A. Banks, A. Mehta, J. Rantus, T. Emmerzaal, T. Kozicz, K. Howell, J. Charlesworth, T. Christensen, Y. Kawaoka, L. Cooper, M. Ackerman, R. Cattaneo, (Research Square preprint), v1, **2020**.
[32] D. E. Rassier, *Am. J. Physiol.: Cell Physiol.* **2017**, *313*, C134.
[33] S. Kurtenbach, S. Kurtenbach, G. Zoidl, *Front. Physiol.* **2014**, *5*, 82.
[34] M. Z. Totland, N. L. Rasmussen, L. M. Knudsen, E. Leithe, *Cell. Mol. Life Sci.* **2020**, *77*, 573.
[35] B. S. Cummings, R. G. Schnellmann, *Curr. Protoc. Pharmacol.* **2004**, *25*, 12.8.1.
[36] Y. Farouz, Y. Chen, A. Terzic, P. Menasché, *Stem Cells* **2015**, *33*, 1021.
[37] M. Kitsara, O. Agbulut, D. Kontziampasis, Y. Chen, P. Menasché, *Acta Biomater.* **2017**, *48*, 20.
[38] P. Joanne, M. Kitsara, S.-E. Boitard, H. Naemetalla, V. Vanneaux, M. Pernot, J. Larghero, P. Forest, Y. Chen, P. Menasché, O. Agbulut, *Biomaterials* **2016**, *80*, 157.
[39] Y. Orlova, N. Magome, L. Liu, Y. Chen, K. Agladze, *Biomaterials* **2011**, *32*, 5615.
[40] J. Li, I. Minami, M. Shiozaki, L. Yu, S. Yajima, S. Miyagawa, Y. Shiba, N. Morone, S. Fukushima, M. Yoshioka, S. Li, J. Qiao, X. Li, L. Wang, H. Kotera, N. Nakatsuji, Y. Sawa, Y. Chen, L. Liu, *Stem Cell Rep.* **2017**, *9*, 1546.
[41] P. Beauchamp, C. B. Jackson, L. C. Ozhathil, I. Agarkova, C. L. Galindo, D. B. Sawyer, T. M. Suter, C. Zuppinger, *Front. Mol. Biosci.* **2020**, *7*, 14.
[42] P. Hoang, A. Kowalczewski, S. Sun, T. S. Winston, A. M. Archilla, S. M. Lemus, A. G. Ercan-Sencicek, A. R. Gupta, W. Liu, M. I. Kontaridis, J. D. Amack, Z. Ma, *Stem Cell Rep.* **2021**, *16*, 1228.
[43] S. George, A. C. Pal, J. Gagnon, S. Timalsina, P. Singh, P. Vydyam, M. Munshi, J. E. Chiu, I. Renard, C. A. Harden, I. M. Ott, A. E. Watkins, C. B. F. Vogels, P. Lu, M. Tokuyama, A. Venkataraman, A. Casanovas-Massana, A. L. Wyllie, V. Rao, M. Campbell, S. F. Farhadian, N. D. Grubaugh, C. S. Dela Cruz, A. I. Ko, A. Z. Berna Perez, E. H. Akaho, D. G. Moledina, J. Testani, A. R. John, M. Ledizet, *Kidney360* **2021**, *2*, 924.
[44] I. O. Osman, C. Melenotte, P. Brouqui, M. Million, J.-C. Lagier, P. Parola, A. Stein, B. L.a Scola, L. Meddeb, J.-L. Mege, D. Raoult, C. A. Devaux, *Front. Immunol.* **2021**, *12*, 625732.
[45] E. S. Kim, M.-T. Jeon, K.-S. Kim, S. Lee, S. Kim, D.-G. Kim, *Viruses* **2021**, 13.
[46] Z. Wen, Y. Zhang, Z. Lin, K. Shi, Y. Jiu, *J. Mol. Cell Biol.* **2020**, *12*, 968.
[47] J. Chen, J. Fan, Z. Chen, M. Zhang, H. Peng, J. Liu, L. Ding, M. Liu, C. Zhao, P. Zhao, S. Zhang, X. Zhang, J. Xu, *Proc. Natl. Acad. Sci. USA* **2021**, *118*, e2111011118.
[48] M. Prondzynski, M. D. Lemoine, A. T. L. Zech, A. Horváth, V. Di Mauro, J. T. Koivumäki, N. Kresin, J. Busch, T. Krause, E. Krämer, S. Schlossarek, M. Spohn, F. W. Friedrich, J. Münch, S. D. Laufer, C. Redwood, A. E. Volk, A. Hansen, G. Mearini, D. Catalucci, C. Meyer, T. Christ, M. Patten, T. Eschenhagen, L. Carrier, *EMBO Mol. Med.* **2019**, *11*, 11115.
[49] A. Aleksova, G. Gagno, G. Sinagra, A. P. Beltrami, M. Janjusevic, G. Ippolito, A. Zumla, A. L. Fluca, F. Ferro, *Int. J. Mol. Sci.* **2021**, *22*, 4526.
[50] O. Sedan, K. Dolnikov, N. Zeevi-Levin, N. Leibovich, M. Amit, J. Itskovitz-Eldor, O. J. S. C. Binah, *Stem Cells* **2008**, *26*, 3130.
[51] E. L. Lagerqvist, B. A. Finnin, C. W. Pouton, J. M. Haynes, *Stem. Cell Res.* **2011**, *6*, 23.
[52] Q. Gao, P. Wang, Z. Wu, H. Qiu, B. Lin, J. Chen, J. Cen, J. J. b. Zhuang, *Biochem. Biophys. Res. Commun.* **2021**, *552*, 84.
[53] E. Avolio, M. Carrabba, R. Milligan, M. Kavanagh Williamson, A. P. Beltrami, K. Gupta, K. T. Elvers, M. Gamez, R. R. Foster, K. Gillespie, F. Hamilton, D. Arnold, I. Berger, A. D. Davidson, D. Hill, M. Caputo, P. Madeddu, *Clin. Sci.* **2021**, *135*, 2667.